SvedbergOpen
DISSEMINATION OF KNOWLEDGE

International Journal of Artificial Intelligence and Machine Learning

Publisher's Home Page: https://www.svedbergopen.com/

Research Paper Open Access

Predictive Quality Management in Nepalese Integrated Machine Learning and Geospatial Modelling for Urban Flood-Risk Prediction and LULC Forecasting In Nashik City, India

Er. Megha D. Kokate[1*], Dr. Ravi Kant Pareek[2]

[1]*PhD Scholar, Vivekananda Global University, Jaipur, Rajasthan.
[2]Associate Professor, Department of Civil Engineering, Vivekananda Global University, Jaipur, Rajasthan.

Abstract
Urban flood risk in fast-growing river cities is controlled jointly by land-cover transition, terrain, rainfall, drainage persistence, and hydrological data quality. This paper restructures the Nashik City thesis evidence into an integrated machine-learning and geospatial framework. Multi-epoch land-use/land-cover (LULC) maps for 1980-2024, a 2030 scenario, terrain derivatives, precipitation, land-surface temperature, runoff indicators, and 1980-2023 discharge records were analysed. K-nearest neighbours (KNN) provide a transparent classification benchmark, a shallow artificial neural network (ANN) supports nonlinear LULC projection, and a time-aware regression workflow produces discharge scenarios. Built-up cover rises from 3.80% in 1980 to 26.03% in 2024 and 29.12% in 2030, while trees decline from 9.53% to 3.01%. KNN reports 88.435% ten-fold mean accuracy at K=5 and 89.376% at K=31. A separate five-class validation reaches 77.03%, with water and trees recognised well but built-up land poorly detected. ANN validation accuracy increases from about 70.3% to 77.3%. Forecasts reproduce monsoon seasonality and report a 6,820 m3/s peak on 19 July 2025. Negative gauge values, gaps, class imbalance, absent uncertainty intervals, and unreported hydraulic calibration restrict operational use. The resulting 4D architecture links geospatial products to explicit historical and forecast dates for auditable planning support.

Keywords: artificial neural network; flood risk; geospatial modelling; K-nearest neighbours; land-use/land-cover; Nashik; remote sensing; time-series forecasting.

Introduction

Urbanisation beside the Godavari River changes the rainfall-runoff response by replacing vegetation and open soil with roofs, roads, and compacted surfaces. In Nashik, this transition increases impervious connectivity, shortens concentration time, intensifies runoff peaks, and exposes additional assets along the river corridor. Long-term remote sensing can quantify the transformation, while machine learning can learn relationships among spectral, terrain, rainfall, runoff, and discharge variables. The planning problem is therefore not simply to make a map; it is to construct a validated sequence linking historical change, present susceptibility, and dated future scenarios [1]-[5].

The study has three objectives: (i) quantify LULC change from 1980 to 2024 and evaluate a 2030 projection; (ii) audit the reported KNN and ANN experiments using fold accuracy, confusion matrices, precision, recall, and F1-score; and (iii) organize runoff and discharge variables into a time-aware forecasting workflow. In this paper, 4D means georeferenced surfaces connected to explicit time steps. It does not imply a fully calibrated hydraulic animation, because water-depth, velocity, and inundation observations required for that claim are not reported.

2. Related Work

Recent watershed research shows that LULC change must be represented explicitly in urban flood analysis [1], [6]-[8]. Machine-learning reviews identify KNN, random forests, neural networks, and deep spatial models as useful for LULC mapping, but also warn that random pixel splits can leak spatial information and that aggregate accuracy can conceal minority-class failure [2], [3], [9], [10]. Multi-epoch studies along Indian growth corridors demonstrate the value of consistent image preprocessing and comparable class legends [11]. Hydrological applications further show that climate forcing and land transformation should be tested jointly rather than inferred from map appearance alone [12], [13].

Systematic remote-sensing reviews emphasize sensor choice, atmospheric correction, seasonal compositing, resolution, and independent validation [14], while global assessments document persistent conversion of natural surfaces into managed and built land [15]. Such transitions modify ecosystem services [16], river morphology [17], water quality [18], [19], and the reliability of data-driven predictions. ANN studies in the Godavari context support nonlinear modelling [20], whereas standard GIS workflows remain essential for reproducibility [21]. Nashik temperature studies show that thermal contrast can help identify exposed and impervious surfaces [22], [23].

Basin-scale multi-criteria water-stress mapping [24], hydrogeochemical analysis [25], landscape-water-quality studies [26], and contemporary reviews [27] support integrated environmental modelling. Scenario LULC projections extend this logic to ecosystem services [28], remote-sensing water-quality assessment [29], and freshwater conservation [30]. The remaining gap is evidential: visually plausible outputs are often presented without separating experiments, checking class balance, blocking spatial or temporal validation, or quantifying forecast uncertainty. This paper addresses that gap by retaining the source results while making their assumptions, calculation context, and limits explicit.

3. Research Methodology

The workflow separates spatial classification, land-transition projection, and discharge forecasting before integrating their outputs. Landsat-derived LULC epochs provide the long-term urban signal; DEM derivatives describe runoff routing; rainfall, runoff, and discharge histories provide temporal predictors; and validation is matched to the dependence structure of each task.

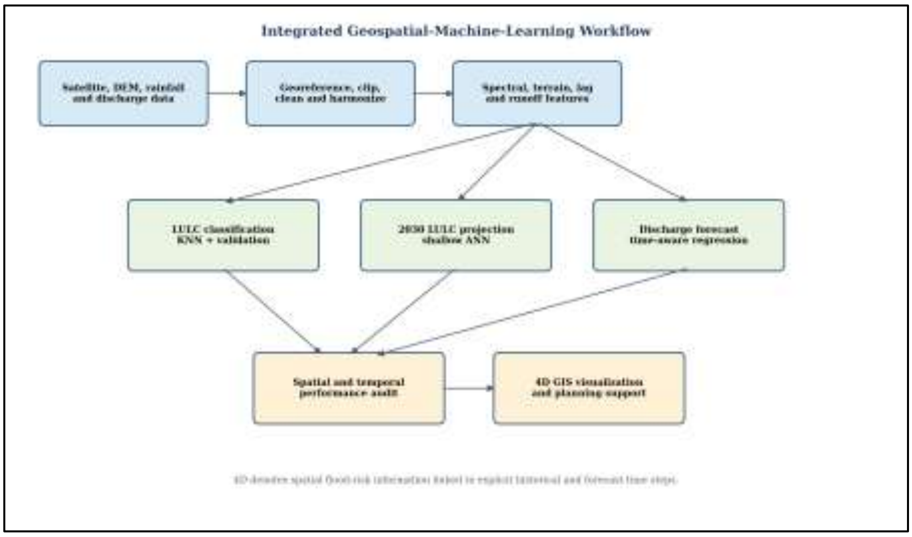

Fig. 1. Integrated research methodology and 4D decision-support workflow.

Source: Reproduced from the submitted Nashik flood-risk thesis report.

Interpretation: The flowchart establishes three modelling branches with a common data foundation but distinct validation rules. Satellite imagery and terrain derivatives feed pixel-level LULC classification; historical LULC states feed the ANN transition learner; and rainfall, runoff, and lagged discharge feed temporal regression. Separating the branches prevents a score from one experiment being attributed to another. Spatially blocked validation is the preferred test for maps because neighbouring pixels are spectrally correlated. Rolling-origin or blocked validation is preferred for discharge because future observations must never influence earlier training. Integration occurs only after these audits, when dated class probabilities, terrain susceptibility, and forecast discharge are registered in the 4D GIS. The architecture also locates the main improvements: representative urban samples belong in the classification branch; uncertainty intervals and hydrological skill scores belong in the forecasting branch; and water-depth and extent observations belong in a later hydraulic calibration branch. Thus the diagram functions as a reproducibility map, not merely a presentation sequence.

Table 1. Data layers, temporal coverage, and analytical role.

Layer	Coverage	Role
LULC	1980-2024; 2030 scenario	Historical transition and urban-growth projection
DEM derivatives	Static terrain grid	Slope, relief, roughness, routing susceptibility
Rainfall and thermal data	Spatial and dated scenes	Forcing and impervious/exposed-surface diagnostics
Hydrological record	1980-2023	Lag, runoff, correlation, and discharge modelling

Layer	Coverage	Role
Forecast series	2025-2030	Monthly/daily scenario and peak identification

Interpretation: The table shows why a single preprocessing rule cannot be applied to every input. LULC epochs are sparse but extend across decades, so they reveal structural urban transition rather than event-scale dynamics. DEM derivatives are effectively static controls and must be resampled consistently with the imagery. Rainfall and land-surface temperature differ in observation date, resolution, and physical meaning; they can enrich interpretation only after coordinate, scale, and timing checks. Hydrological records are comparatively frequent and support lagged features, yet their usefulness depends on quality control for gaps and non-physical readings. Forecasts are model outputs, not observations, and must remain labelled as scenarios. The combined design supports three linked but separately auditable tasks: categorical map classification, nonlinear land-transition learning, and continuous discharge prediction. This distinction justifies the use of different metrics and split strategies. It also prevents 2030 LULC and 2025-2030 discharge products from being mistaken for measured environmental states.

4. Mathematical Modelling and Design

Fig. 2. Model design for LULC classification, ANN transition learning, and discharge forecasting.
Source: Reproduced from the submitted Nashik flood-risk thesis report.

Interpretation: The design diagram clarifies the different mathematical objects produced by the models. KNN operates on a scaled feature vector and assigns a pixel class using distances to labelled neighbours; it has no training epochs. The ANN instead transforms historical state vectors through learned nonlinear weights and produces class probabilities, so its loss and validation accuracy can be monitored by epoch. Hydrological regression maps rainfall, runoff, seasonal, and lagged-discharge features to a continuous predicted flow value. These outputs should not be evaluated with one common score: LULC requires class-wise precision, recall, F1-score, and confusion matrices, whereas discharge requires time-ordered error and hydrological skill statistics. The final 4D layer stores predictions with coordinates, timestamps, and model metadata. It can support scenario comparison, but reliable operational alerts additionally require calibration against observed event hydrographs and inundation extents. The model design therefore supplies a disciplined interface between data, algorithms, outputs, validation, and decision use.

$$z_j = (x_j - \mu_j) / \sigma_j \qquad (1)$$

$$d(x,x_i) = [\Sigma_j (z_j - z_{ij})^2]^{(1/2)}; \quad \hat{y} = \mathrm{mode}\{y_i : i \in N_K(x)\} \qquad (2)$$

$$h = g(W_1x+b_1); \quad p(c|x) = \mathrm{softmax}(W_2h+b_2) \qquad (3)$$

$$L_{CE} = -(1/N)\ \Sigma_i\ \Sigma_c\ y_{ic} \log p_{ic} \qquad (4)$$

$$\hat{Q}_t = f(P_t, R_t, R_{(t-1:t-L)}, Q_{(t-1:t-L)}, S_t, U_t) \qquad (5)$$

Here x is the predictor vector, z is its standardized form, $N_K(x)$ is the K-neighbourhood, h is the hidden ANN representation, $p(c|x)$ is class probability, and $\hat{Q}_t$ is predicted discharge. P, R, S, and U denote rainfall, runoff, seasonal encoding, and land-cover/urban variables. Scaling parameters must be estimated from training data only.

Table 2. Reported model calculations and validation evidence.

Experiment	Calculation	Result
KNN, K=5	mean of 10 fold accuracies	0.88435
K sweep	max mean accuracy at K=31	0.893764
KNN holdout	0.9018 train - 0.8970 test	0.0048 gap
Five-class pixels	12,542 / 16,282	0.7703
ANN epochs	0.773 - 0.703	+0.070

Interpretation: The calculations show that the source report contains several legitimate but non-equivalent evaluations. The ten-fold KNN mean at K=5 is 0.88435. Increasing the neighbourhood to K=31 raises the reported mean to 0.893764, an absolute gain of 0.009414, or about 0.94 percentage points. A separate feature-table split produces 0.9018 training and 0.8970 test accuracy; the 0.0048 gap suggests limited conventional overfitting within that split but does not test spatial transfer. The five-class confusion matrix contains 12,542 correct pixels among 16,282, giving 0.7703 overall accuracy. Finally, ANN validation accuracy improves from approximately 0.703 to 0.773, a seven-percentage-point increase across epochs. These values must remain attached to their sample definitions, algorithms, and partitions. Their differences are evidence about validation context, not contradictory measurements of one universal model. Deployment claims require spatially disjoint map testing and time-ordered discharge testing beyond these reported results. This interpretation preserves transparency across the report's otherwise heterogeneous experimental evidence.

5. Results and Discussion

5.1 LULC transition and 2030 scenario

Table 3. LULC composition and calculated change (percent of mapped area).

Class	1980	2024	2030	1980-2030 change
Crops	46.80	41.97	43.13	-3.67 pp
Rangeland	36.50	27.02	23.44	-13.06 pp
Trees	9.53	3.19	3.01	-6.52 pp
Built-up	3.80	26.03	29.12	+25.32 pp
Water	3.37	1.79	1.30	-2.07 pp

Interpretation: The table quantifies a strong transition from permeable and vegetated land toward urban cover. Built-up land increases from 3.80% in 1980 to 26.03% in 2024 and 29.12% in the 2030 scenario. The 25.32-percentage-point rise equals 7.66 times the 1980 baseline. Rangeland loses 13.06 points, tree cover loses 6.52 points, water loses 2.07 points, and crops decline by 3.67 points across 1980-2030. The five classes sum to 100% in each reported year, supporting internal compositional consistency. Hydrologically, the direction of change implies reduced interception and infiltration, greater connected impervious area, and faster runoff delivery, although peak-flow change cannot be calculated from area fractions alone. The projected 2030 values are scenario outputs and therefore inherit classification and transition uncertainty. Because built-up recognition is weak in the five-class validation, its trend should be confirmed with targeted urban samples and independent imagery before parcel-scale regulation or drainage design decisions.

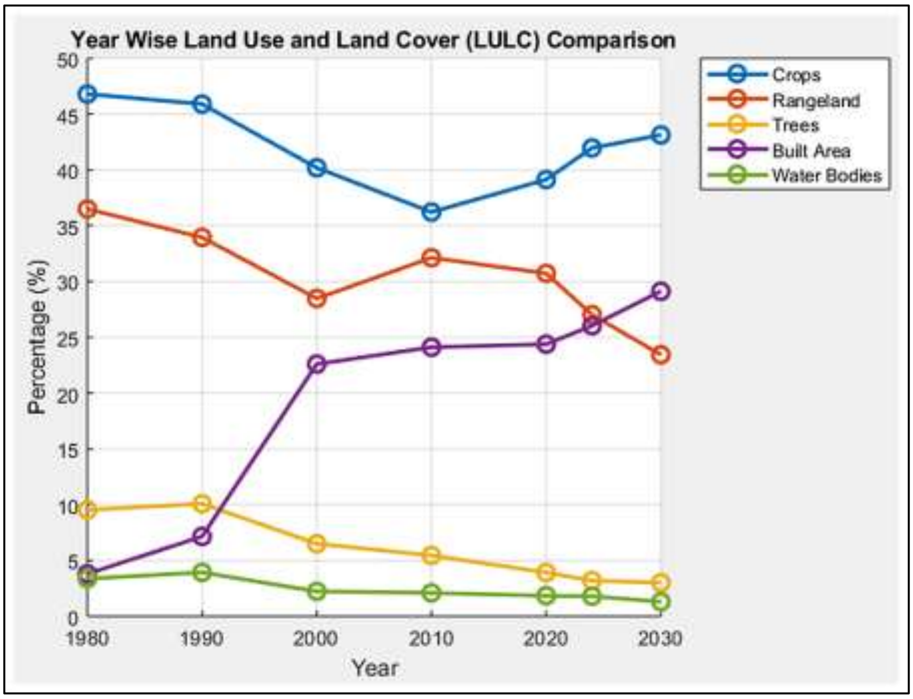

Fig. 3. Year-wise LULC comparison, 1980-2030.

Source: Reproduced from the submitted Nashik flood-risk thesis report.

Interpretation: The chart exposes the temporal structure behind the endpoint calculation. Built-up land grows slowly in the early decades and accelerates in the recent urban period, while rangeland and tree cover generally contract. Cropland remains the largest class but fluctuates, indicating that urban expansion is not supplied by one land category alone. Water-body decline is smaller in absolute area share yet important because river and wetland surfaces influence storage, conveyance, habitat, and floodplain connectivity. The 2030 bars extend the observed direction rather than constituting direct measurements. Their plausibility depends on consistent class definitions, comparable seasonal imagery, representative transition samples, and stable drivers. The figure therefore supports a planning narrative of rising imperviousness, but not a deterministic prediction of inundation depth. For flood-risk use, each epoch should be accompanied by class probabilities and change-detection confidence. The largest priority is built-up validation, because misclassification of impervious surfaces propagates directly into runoff assumptions and urban-growth scenarios.

5.2 ANN learning behaviour

The shallow ANN learns nonlinear transition relationships among historical LULC states. Its training history is interpreted independently from KNN because KNN is tuned by neighbourhood size rather than gradient-based epochs.

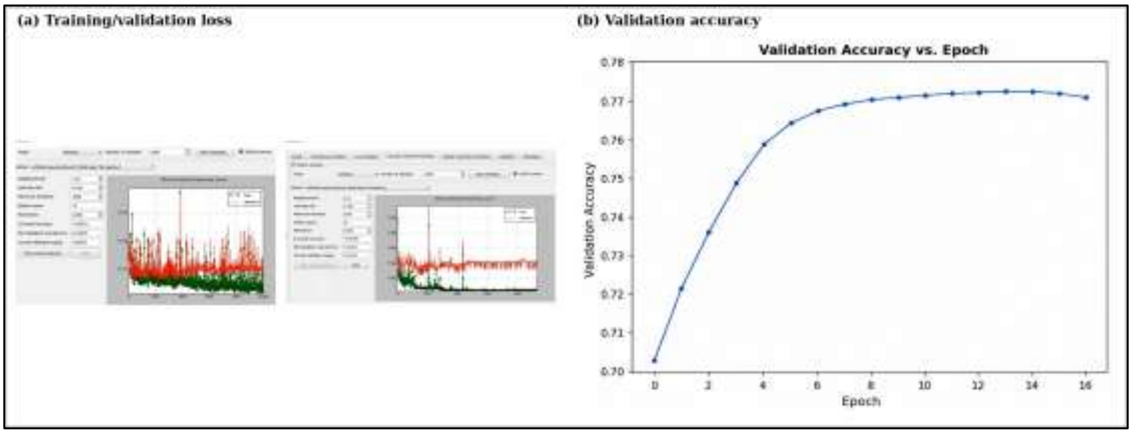

Fig. 4. ANN loss behaviour and validation-accuracy convergence.

Source: Reproduced from the submitted Nashik flood-risk thesis report.

Interpretation: The paired loss curves show early oscillation followed by a more stable decline, while validation loss remains above training loss, as expected for unseen data. The accompanying accuracy curve rises from approximately 0.703 at epoch 0 to about 0.773 near epoch 13. The absolute increase is 0.070, and the relative improvement over the starting value is approximately 9.96%. Most gain occurs during the first eight epochs; later changes are small, and the final value near 0.771 is only 0.002 below the reported maximum. This pattern supports early stopping around epochs 12-14, provided the monitored set is spatially independent. Convergence does not by itself establish spatial transferability because neighbouring pixels can make validation artificially easy. The ANN result is therefore evidence of stable optimisation, not proof that the projected 2030 map is error-free. Repeated seeds, blocked spatial validation, class-balanced loss, and probability calibration would strengthen the projection and quantify sensitivity to initialization and sampling.

Design implication

The ANN should store the selected epoch, random seed, normalization parameters, class weights, and transition probabilities. Early stopping controls unnecessary training, while class-balanced sampling reduces dominance by common surfaces. For scenario use, uncertainty can be represented through repeated model runs or ensembles and propagated into mapped class-probability ranges.

Model separation

The ANN maximum near 77.3% is not directly comparable with the KNN values near 88-89% because the algorithms, outputs, partitions, and likely sample supports differ. Presenting the scores as separate experiments is essential for technical correctness and prevents a misleading ranking based only on headline accuracy.

5.3 KNN cross-validation and neighbourhood selection

KNN assigns each standardized feature vector from the labels of nearby training samples. The source report provides a ten-fold experiment at K=5 and a second sweep over larger odd K values.

Fig. 5. KNN ten-fold performance at K=5 and neighbourhood-size sweep.

Source: Reproduced from the submitted Nashik flood-risk thesis report.

Interpretation: At K=5, ten-fold accuracies range from about 0.8606 to 0.9571 and average 0.88435, giving a spread of roughly 9.65 percentage points. The variation shows that performance depends on fold composition and should not be reduced to one split. The K sweep reports 0.8924 at K=21, 0.8928 at 23, 0.8937 at 25, 0.8932 at 27, 0.8935 at 29, a maximum of 0.893764 at 31, and about 0.8935 at 33. Compared with K=5, the best gain is approximately 0.00941, or 0.94 percentage points. The flat plateau means K values from roughly 25-33 are operationally similar; selecting K=31 solely from the fourth decimal place would overstate precision. Model choice should additionally consider macro-F1, minority recall, probability calibration, computational cost, and spatially blocked folds. Random pixel folds remain optimistic when neighbouring samples share spectral and terrain characteristics. This modest improvement must also be tested across alternative spatial partitions and years.

Holdout evidence

A separate feature-table experiment reports 0.9018 training accuracy and 0.8970 test accuracy. The 0.0048 gap is small, suggesting limited overfitting under that partition. However, the dominant confusion-matrix diagonal and different sample support show that this experiment is not the same as the five-class evaluation on the next page. Its result should be labelled with its own split and dataset.

Recommended configuration

Use standardized continuous features, odd K values, distance weighting where justified, and nested selection so K is chosen without viewing the final test data. Report fold mean and dispersion, class-wise metrics, and a spatially disjoint holdout. The reported K=31 setting is a defensible candidate, while K=5 remains a transparent local baseline.

5.4 Five-class validation and error structure

The class-level evaluation is the decisive audit for flood-planning use because aggregate accuracy can remain acceptable even when impervious urban land is poorly detected.

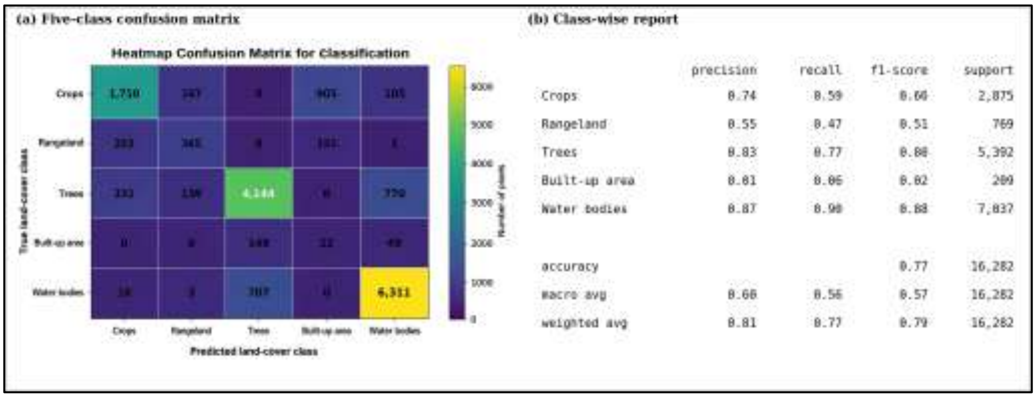

Fig. 6. Five-class LULC confusion matrix and classification report.

Source: Reproduced from the submitted Nashik flood-risk thesis report.

Interpretation: The matrix contains 16,282 validation pixels, with 12,542 correct diagonal classifications; overall accuracy is therefore 12,542/16,282 = 0.7703, or 77.03%. Water and trees dominate the reliable predictions, contributing 6,311 and 4,144 correct pixels. Water achieves precision 0.87, recall 0.90, and F1 0.88; trees achieve 0.83, 0.77, and 0.80. Crops are moderate at F1 0.66 and rangeland reaches 0.51. Built-up land is the critical failure, with precision 0.01, recall 0.06, F1 0.02, and only 12 correct pixels. Macro-F1 is 0.57, far below weighted-F1 0.79 because high-support classes dominate weighting. Errors include 905 crop pixels labelled built-up and strong water-tree confusion. Since impervious cover is a major runoff driver, urban under-detection can bias risk scenarios. Targeted urban sampling, texture/context features, multispectral indices, class-balanced loss, and independent spatial validation are required before regulatory use. Probability calibration should also be assessed because planning systems consume confidence values, not labels alone.

Planning interpretation

The map products are suitable for research-level comparison and scenario screening, not parcel-scale enforcement. A confidence mask should accompany the mapped classes, and urban-growth statistics should be recalculated after improving built-up recall. Water and tree performance is promising, but their confusion should be examined along riparian and mixed-pixel boundaries where floodplain interpretation is most sensitive.

Metric policy

Future reporting should prioritize macro-F1, built-up recall, balanced accuracy, and area-adjusted accuracy alongside the usual overall score. Validation polygons should be geographically separated from training areas and stratified across urban form, riparian corridors, agriculture, shadow, and mixed land cover. This policy aligns model selection with flood-risk consequences rather than class prevalence.

5.5 Hydrologic feature diagnostics and prediction behaviour

Hydrological analysis combines calendar variables, discharge, flood runoff, daily runoff, and weekly runoff. Correlation is used only as a linear diagnostic; time dependence, lag structure, and nonlinear thresholds require supervised evaluation.

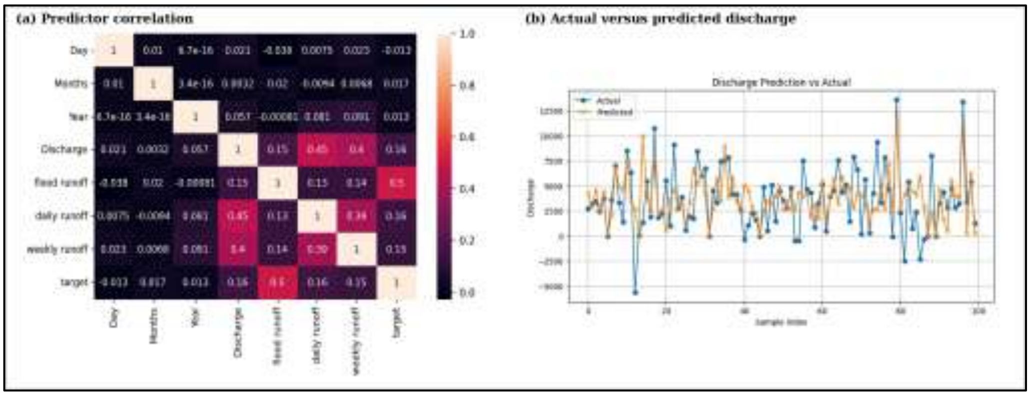

Fig. 7. Hydrological predictor correlation and actual-versus-predicted discharge.

Source: Reproduced from the submitted Nashik flood-risk thesis report.

Interpretation: The correlation panel identifies flood runoff as the strongest linear associate of the target at 0.50. Discharge relates to daily and weekly runoff at about 0.45 and 0.40, whereas raw day, month, and year variables have near-zero target correlations. This supports hydrological histories and seasonal encodings over untransformed calendar indices, while the intercorrelations among runoff features also warn of redundancy. In the actual-versus-predicted panel, the model follows central movement but under-represents several extreme peaks above roughly 10,000 m3/s. Observations also include negative discharge values near -5,500 and -2,500 m3/s, which are physically implausible for ordinary river flow and likely represent missing-value codes, datum problems, or preprocessing errors. These values must be investigated rather than silently clipped. Because RMSE, MAE, Nash-Sutcliffe efficiency, and prediction intervals are not reported, they are not invented here. A defensible forecast requires quality-controlled targets, time-ordered testing, peak-sensitive loss, baseline comparison, and uncertainty bands.

Data-quality controls
Every gauge record should carry provenance and quality flags. Suspect negative values, gaps, duplicated timestamps, unit changes, and rating-curve revisions should be reconciled with station metadata. Missing observations may be imputed only within a documented validation experiment; otherwise they should be excluded from target fitting. All lag and rolling variables must be generated causally so future discharge cannot leak into earlier predictions.

Required hydrological metrics
Future evaluation should report MAE, RMSE, bias, R^2, Nash-Sutcliffe efficiency, Kling-Gupta efficiency, peak timing error, peak magnitude error, and performance by monsoon phase. A seasonal-naive baseline and a persistence baseline are essential. Prediction intervals should be checked for empirical coverage, especially during high-flow events that drive planning decisions.

5.6 Scenario discharge, planning use, and limitations

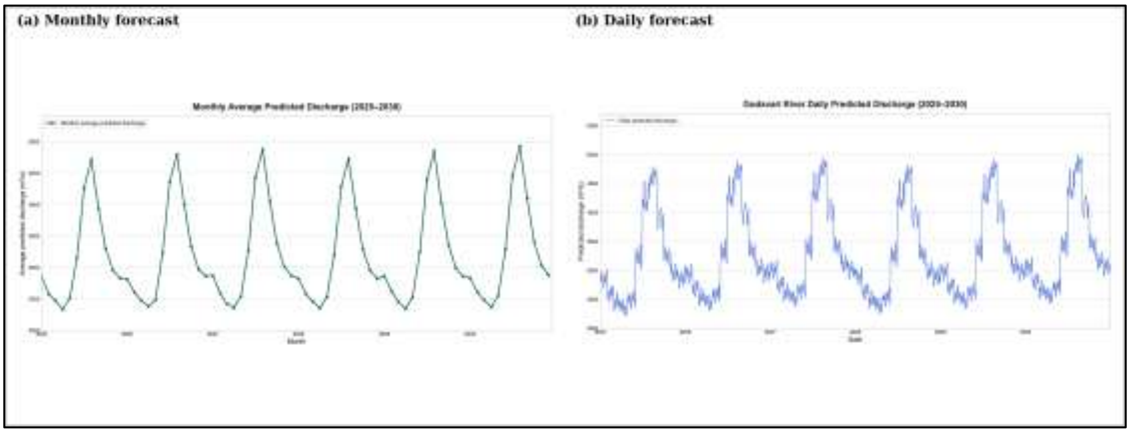

Fig. 8. Monthly and daily predicted discharge scenarios for 2025-2030.
Source: Reproduced from the submitted Nashik flood-risk thesis report.

Interpretation: Both panels reproduce a pronounced annual monsoon cycle. Monthly averages rise from dry-season levels near 2,300-3,000 m3/s toward yearly peaks of roughly 4,700-4,900 m3/s, while the daily curve preserves shorter fluctuations and peaks near 5,000 m3/s in the displayed series. A separate peak table in the source report identifies a scenario maximum of 6,820 m3/s on 19 July 2025. The repeated seasonal shape is plausible but may reflect strong calendar or templated forcing; it does not demonstrate skill beyond the historical test period. Interannual variation is limited, and no climate ensemble, prediction interval, hydraulic threshold, or calibrated inundation relationship is supplied. The outputs should therefore be treated as planning scenarios for scheduling drainage inspection, riparian monitoring, and emergency preparedness, not as deterministic warnings. Operational deployment requires updated rainfall forecasts, gauge assimilation, rolling retraining, uncertainty calibration, threshold validation, and comparison with persistence and seasonal-naive baselines. Forecast dates must remain linked to model version and data provenance in the 4D GIS.

6. Conclusion

The integrated analysis demonstrates substantial urban transformation in Nashik and provides a technically consistent account of the reported machine-learning evidence. Built-up cover rises by 25.32 percentage points from 1980 to the 2030 scenario, while rangeland, trees, and water decline. KNN reaches a reported ten-fold mean of 88.435% at K=5 and 89.376% at K=31; the small gain and fold spread argue for spatial validation rather than fine-grained tuning claims. The separate five-class test reaches 77.03% overall accuracy but reveals unacceptable built-up F1 of 0.02. ANN learning stabilizes near 77.3% validation accuracy. Hydrological forecasts reproduce seasonal structure, yet negative observations, data gaps, muted peaks, and missing uncertainty measures constrain confidence.

The practical contribution is a 4D decision-support structure in which LULC, terrain, hydrological diagnostics, and dated scenarios remain traceable to their models and validation evidence. Before operational use, future work should improve urban samples, use spatially blocked classification tests, clean and document the gauge record, perform rolling-origin forecasting, report hydrological skill and prediction intervals, and calibrate water depth and inundation extent against observed events. With these controls, the framework can support drainage investment, riparian protection, growth regulation, and transparent flood preparedness.

Limitations

The study is constrained by heterogeneous source experiments, uncertain negative gauge codes, unreported forecast residual metrics, and the absence of independent inundation observations. Consequently, it justifies model-development and scenario conclusions but does not claim real-time warning reliability or parcel-scale hydraulic accuracy.

References

1. M. Banjara, A. Bhusal, A. B. Ghimire, and A. Kalra, 'Impact of land use and land cover change on hydrological processes in urban watersheds: Analysis and forecasting for flood risk management,' Geosciences, vol. 14, no. 2, Art. no. 40, 2024, doi: 10.3390/geosciences14020040.
2. J. Wang, M. Bretz, M. A. A. Dewan, and M. A. Delavar, 'Machine learning in modelling land-use and land cover-change (LULCC): Current status, challenges and prospects,' Sci. Total Environ., vol. 822, Art. no. 153559, 2022, doi: 10.1016/j.scitotenv.2022.153559.
3. V. Pushpalatha, P. B. Mallikarjuna, H. N. Mahendra, S. Rama Subramoniam, and S. Mallikarjunaswamy, 'Land use and land cover classification for change detection studies using convolutional neural network,' Appl. Comput. Geosci., vol. 25, Art. no. 100227, 2025, doi: 10.1016/j.acags.2025.100227.
4. R. Ande et al., 'Understanding climate change impacts on streamflow by using machine learning: Case study of Godavari Basin,' Water, vol. 17, no. 8, Art. no. 1171, 2025, doi: 10.3390/w17081171.
5. J. Mukherjee and S. Ghosh, 'Decoding the vitality of Earth observation for flood monitoring in the Lower Godavari River Basin, India,' J. Geol. Soc. India, vol. 99, no. 6, pp. 802-808, 2023, doi: 10.1007/s12594-023-2387-9.
6. M. Aher and S. M. Yadav, 'Effect of land use and land cover change on spatial and temporal variation of hydrological parameters of Godavari River Basin, India,' Theor. Appl. Climatol., vol. 156, Art. no. 65, 2025, doi: 10.1007/s00704-024-05288-9.
7. K. Sharma, R. Tiwari, A. K. Wadhwani, and S. Chaturvedi, 'Evaluating the impact of land use land cover changes on urban ecosystem services in Nashik, India: An RS-GIS based approach,' Environ. Earth Sci., vol. 83, Art. no. 683, 2024, doi: 10.1007/s12665-024-11965-9.
8. P. Saraf and D. G. Regulwar, 'Land use land cover analysis for Godavari Basin in Maharashtra using geographical information system and remote sensing,' J. Geogr. Inf. Syst., vol. 16, no. 1, pp. 21-31, 2024, doi: 10.4236/jgis.2024.161002.
9. S. Gaur and R. Singh, 'A comprehensive review on land use/land cover change modeling for urban development: Current status and future prospects,' Sustainability, vol. 15, no. 2, Art. no. 903, 2023, doi: 10.3390/su15020903.
10. C. Rong and W. Fu, 'A comprehensive review of land use and land cover change based on knowledge graph and bibliometric analyses,' Land, vol. 12, no. 8, Art. no. 1573, 2023, doi: 10.3390/land12081573.
11. A. Kanchan, V. Nitivattananon, N. K. Tripathi, E. Winijkul, and R. R. Mandadi, 'A spatio-temporal examination of land use and land cover changes in smart cities of the Delhi-Mumbai Industrial Corridor,' Land, vol. 13, no. 7, Art. no. 957, 2024, doi: 10.3390/land13070957.
12. M. Kumar, D. M. Denis, A. Kundu, N. Joshi, and S. Suryavanshi, 'Understanding land use/land cover and climate change impacts on hydrological components of Usri watershed, India,' Appl. Water Sci., vol. 12, Art. no. 39, 2022, doi: 10.1007/s13201-021-01547-6.
13. M. Moniruzzaman et al., 'Decadal urban land use/land cover changes and its impact on surface runoff potential for Dhaka City and surroundings using remote sensing,' Remote Sens., vol. 13, no. 1, Art. no. 83, 2021, doi: 10.3390/rs13010083.
14. M. J. Mashala, T. Dube, B. T. Mudereri, K. K. Ayisi, and M. R. Ramudzuli, 'A systematic review on advancements in remote sensing for assessing and monitoring land use and land cover change impacts on surface water resources in semi-arid tropical environments,' Remote Sens., vol. 15, no. 16, Art. no. 3926, 2023, doi: 10.3390/rs15163926.
15. G. A. Afuye et al., 'Global trend assessment of land use and land cover changes: A systematic approach to future research development and planning,' J. King Saud Univ. Sci., vol. 36, no. 7, Art. no. 103262, 2024, doi: 10.1016/j.jksus.2024.103262.
16. S. S. Hasan, L. Zhen, M. G. Miah, T. Ahamed, and A. Samie, 'Impact of land use change on ecosystem services: A review,' Environ. Dev., vol. 34, Art. no. 100527, 2020, doi: 10.1016/j.envdev.2020.100527.

17. N. M. Kayitesi, A. C. Guzha, and G. Mariethoz, 'Impacts of land use land cover change and climate change on river hydro-morphology: A review of research studies in tropical regions,' J. Hydrol., vol. 615, Art. no. 128702, 2022, doi: 10.1016/j.jhydrol.2022.128702.
18. S. Navasakthi et al., 'Assessment of spatial and temporal variation in water quality for the Godavari River,' Water, vol. 15, no. 17, Art. no. 3076, 2023, doi: 10.3390/w15173076.
19. A. C. Kharake and V. S. Raut, 'An assessment of water quality index of Godavari River water in Nashik City, Maharashtra,' Appl. Water Sci., vol. 11, Art. no. 101, 2021, doi: 10.1007/s13201-021-01432-2.
20. N. Satish, J. Anmala, R. K., and M. R. R. Varma, 'Prediction of stream water quality in Godavari River Basin, India using statistical and artificial neural network models,' H2Open J., vol. 5, no. 4, pp. 621-641, 2022, doi: 10.2166/h2oj.2022.019.
21. Q. Sultana, A. Sultana, and Z. Ara, 'Assessment of the land use and landcover changes using remote sensing and GIS techniques,' in Water, Land, and Forest Susceptibility and Sustainability, Elsevier, 2023, pp. 267-297, doi: 10.1016/B978-0-323-91880-0.00022-2.
22. A. Dhorde and S. Deka, 'Changes in land use and land surface temperature over Nashik City, MS, India,' in Research Developments in Geotechnics, Geo-Informatics and Remote Sensing, Springer, 2022, pp. 395-399, doi: 10.1007/978-3-030-72896-0_90.
23. K. Gadekar, C. B. Pande, J. Rajesh, S. D. Gorantiwar, and A. A. Atre, 'Estimation of land surface temperature and urban heat island by using Google Earth Engine and remote sensing data,' in Climate Change Impacts on Natural Resources, Ecosystems and Agricultural Systems, Springer, 2023, pp. 367-389, doi: 10.1007/978-3-031-19059-9_14.
24. S. Sarkar, 'Appraisal of water stress regions of Godavari Basin for climate resilient water resource management: A GIS-MCDA based approach,' J. Earth Syst. Sci., vol. 132, Art. no. 182, 2023, doi: 10.1007/s12040-023-02196-w.
25. C. B. Pande et al., 'Implications of seasonal variations of hydrogeochemical analysis using GIS, WQI, and statistical analysis method for the semi-arid region,' Appl. Water Sci., vol. 15, Art. no. 80, 2025, doi: 10.1007/s13201-025-02387-4.
26. F. Zhang et al., 'Impact of land-use/land-cover and landscape pattern on seasonal in-stream water quality in small watersheds,' J. Clean. Prod., vol. 357, Art. no. 131907, 2022, doi: 10.1016/j.jclepro.2022.131907.
27. K. A. Locke, 'Impacts of land use/land cover on water quality: A contemporary review for researchers and policymakers,' Water Qual. Res. J., 2024, doi: 10.2166/wqrj.2024.002.
28. M. Z. Hoque, S. Cui, I. Islam, L. Xu, and J. Tang, 'Future impact of land use/land cover changes on ecosystem services in the Lower Meghna River Estuary, Bangladesh,' Sustainability, vol. 12, no. 5, Art. no. 2112, 2020, doi: 10.3390/su12052112.
29. M. A. Gani, A. M. Sajib, M. A. Siddik, and M. Moniruzzaman, 'Assessing the impact of land use and land cover on river water quality using water quality index and remote sensing techniques,' Environ. Monit. Assess., vol. 195, Art. no. 449, 2023, doi: 10.1007/s10661-023-10989-1.
30. C. A. Sayer et al., 'One-quarter of freshwater fauna threatened with extinction,' Nature, vol. 638, pp. 138-145, 2025, doi: 10.1038/s41586-024-08375-z.